Beyond the delay barrier in adaptive feedforward active noise control using Youla -Kučera parametrization

Ioan Doré Landau, Raúl Antonio Meléndez, Tudor-Bogdan Airimitoaie, Luc Dugard

▶ **To cite this version:**

Ioan Doré Landau, Raúl Antonio Meléndez, Tudor-Bogdan Airimitoaie, Luc Dugard. Beyond the delay barrier in adaptive feedforward active noise control using Youla -Kučera parametrization. Journal of Sound and Vibration, 2019, 455 (September), pp.339-358. 10.1016/j.jsv.2019.05.028 . hal-02136074

HAL Id: hal-02136074
https://hal.science/hal-02136074v1

Submitted on 21 May 2019

HAL is a multi-disciplinary open access archive for the deposit and dissemination of scientific research documents, whether they are published or not. The documents may come from teaching and research institutions in France or abroad, or from public or private research centers.

L'archive ouverte pluridisciplinaire **HAL**, est destinée au dépôt et à la diffusion de documents scientifiques de niveau recherche, publiés ou non, émanant des établissements d'enseignement et de recherche français ou étrangers, des laboratoires publics ou privés.

Beyond the delay barrier in adaptive feedforward active noise control using Youla –Kučera parametrization

Ioan Doré Landau[a], Raul Melendez[a], Tudor-Bogdan Airimitoaie[a], Luc Dugard[a]

[a] *Univ. Bordeaux, Bordeaux INP, CNRS, IMS, UMR 5218, 33405 Talence, France*
[b] *Univ. Grenoble Alpes, CNRS, Grenoble INP*[1]

Abstract

Adaptive feedforward broad-band noise compensation is currently used when a correlated measurement with the disturbance (an image of the disturbance) is available. Most of the active feedforward noise control systems feature an internal "positive" acoustical feedback between the compensation system and the reference source (a correlated measurement with the disturbance) which has to be taken into account. Adaptive algorithms for active feedforward noise attenuation have been implemented such that the propagation delay between the compensatory actuator and the measurement of the residual noise (the secondary path) be much smaller than the propagation delay between the reference source (image of the incoming noise) and the measurement of the residual noise (the primary path). Nevertheless, there are potential fields of applications where the propagation delay of the secondary path may be larger than the one of the primary path. The present paper explores the behaviour of the available adaptive feedforward compensation algorithms in this new context. The algorithms have been tested experimentally on a relevant test bench. All the algorithms except the Youla–Kučera finite impulse response (YKFIR) adaptive compensator and the standard FIR adaptive compensator using a stability based filtered adaptation (FUSBA) lead to an unstable behavior. In terms of performance the YKFIR provides the best performance.

Keywords: active noise control, adaptive feedforward compensation, Youla–Kučera parametrization, positive feedback coupling

1. Introduction

Adaptive feedforward broad-band noise compensation is currently used when a correlated measurement with the disturbance (an image of the disturbance) is available. Most of the active feedforward noise control systems feature an internal "positive" acoustic feedback between the compensation system and the reference source (a correlated measurement with the disturbance) which has to be taken into account.

Figure 1 gives the basic block diagram of the adaptive feedforward compensation in the presence of the internal positive coupling between the output of the compensator and the measurement

[1]Corresponding author: Ioan Doré Landau Institute of Engineering Univ. Grenoble Alpes, GIPSA-lab, 38000 Grenoble, France (ioan-dore.landau@gipsa-lab.grenoble-inp.fr)

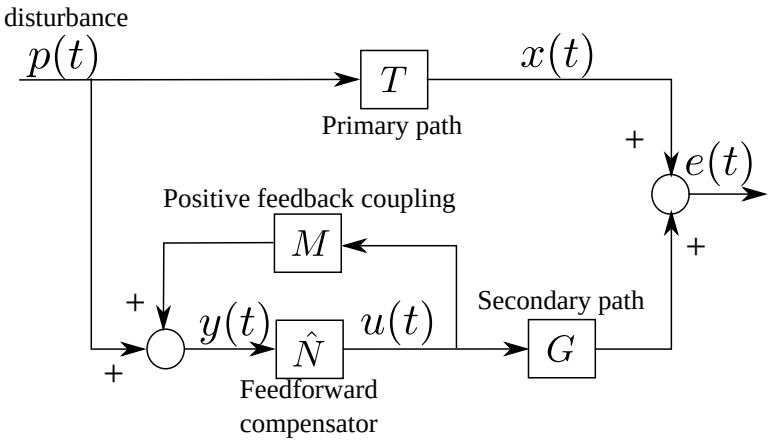

Figure 1: Adaptive active noise feedforward compensation.

of the image of the incoming noise. The incoming noise propagates through the so called *primary path* and its effect is compensated through a secondary noise source (*secondary path*) driven by a feedforward compensator. The input to the feedforward compensator is the sum of the image of the incoming noise and of the internal acoustic positive feedback. Since this feedback is positive, it raises of course stability problems. Stability analysis of the adaptive feedforward compensation schemes became an important issue [1–3]. The stability analysis make the assumption that there exists a compensator N such that the internal positive loop (formed by M and N in feedback) is stable and such that the perfect matching of the primary path is achieved.[2]

One of the important aspects in active noise feedforward control is the transportation delay related to the sound propagation speed [4]. Most of the implementations of the adaptive feedforward compensation systems are close to a collocation of the residual noise measurement and of the secondary source used for compensation (see for example [5],[6]). More generally speaking, the length between these two objects is much smaller than the length of the primary path (between the reference microphone and the residual noise microphone). See for example [7]. A ratio of 3 to 6 seems to be the case in a number of applications (particularly true in the active noise compensation in ducts).

Nevertheless, there are potential applications fields where the length of the secondary path may be longer than the length of the primary path.[3] In this case the delay associated with the dynamics of the secondary path will be larger than the delay associated with the primary path.

When the delay characterizing the dynamic model of the secondary path is larger than the delay of the primary path, even in the absence of the internal positive feedback, it just simply does not exist a stable compensator assuring the "perfect matching"[4]. One needs algorithms which will

[2]This hypothesis of perfect matching of the primary path can be relaxed under certain conditions taking into account that the perfect matching should be achieved in practice in a limited frequency band (see [2]).

[3]This can occur when there are thermal constraints for the positioning of the secondary source.

[4]In the case of the internal feedback the effective compensator is the feedback connection of the compensator N and of the reverse path M.

minimize the residual noise and which will assure the stability of the scheme (and of course the stability of the internal loop). The present paper does not propose new algorithms but tries to evaluate in this context the available algorithms for adaptive feedforward compensation using a relevant experimental test bench.

As it will be shown in this paper, only the adaptive Youla–Kučera (YK) parametrized compensator using a Finite Impulse Response (FIR) filter [3] and the Filtered u stability based algortithm (FUSBA) associated to a standard FIR compensator [2, 8] assure a stable operation of the system. All the other algorithms tested do not assure a stable operation. In terms of performance it is the Youla–Kučera FIR adaptive feedforward compensator which has provided the best performance. The reason for the good behavior of the Youla–Kučera parametrized FIR (YKFIR) algorithm is that from the beginning the internal loop will be stable (by the appropriate design of the central compensator) independently of the values of the parameters of the YKFIR filter which will be adapted in order to minimize the residual noise. The standard FUSBA FIR adaptive compensator provides less good performance and does not offer the possibility to assign the poles of the internal closed-loop which unfortunately go extremely close to the unit circle. This raises questions about its robustness.

All the algorithms have been tested in real-time on a relevant test bench and in simulation using the identified models of the test bench. The performance of the Youla–Kučera FIR algorithm will be thoroughly investigated.

The paper is organized as follows: In Section 2, the experimental setup will be described. In Section 3, the basic equations describing the system will be presented in order to make understandable the various algorithms which will be reviewed in Sections 4 and 5. Section 6 will show simulation results. The experimental results obtained on the test bench are summarized in Section 7. Conclusions are given in Section 8. Appendix A provides an analysis of the possible stable/unstable equilibrium points for the various schemes. Appendix B provides simulation results for a simplified YKFIR adaptive feedforward compensator.

2. Experimental Setup

The view of the test bench used for experiments is shown in Fig. 2 and its detailed scheme is given in Fig. 3. The actual dimensions of the test bench are given in Fig. 4.

The speaker used as the source of disturbances is labelled as 1, while the control speaker is marked as 2. At pipe's open end, the microphone that measures the system's output (residual noise $e(t)$) is denoted as 3. Inside the pipe, close to the source of disturbances, we can find the second microphone, labelled as 4, for measuring the perturbation's image, denoted as $y(t)$. Additionally, we denote $u(t)$ the control signal and $s(t)$ the disturbance. The transfer function between the disturbance's speaker and the microphone ($1\rightarrow3$) is called *Global Primary Path*, while the transfer function between the control speaker and the microphone ($2\rightarrow3$) is denoted *Secondary Path*. The transfer function between microphones ($4\rightarrow3$) is called *Primary Path*. The internal coupling found between ($2\rightarrow4$) is denoted *Reverse Path*. These marked paths have a double differentiator behaviour, since as input we have the voice coil displacement and as output the air acoustic pressure.

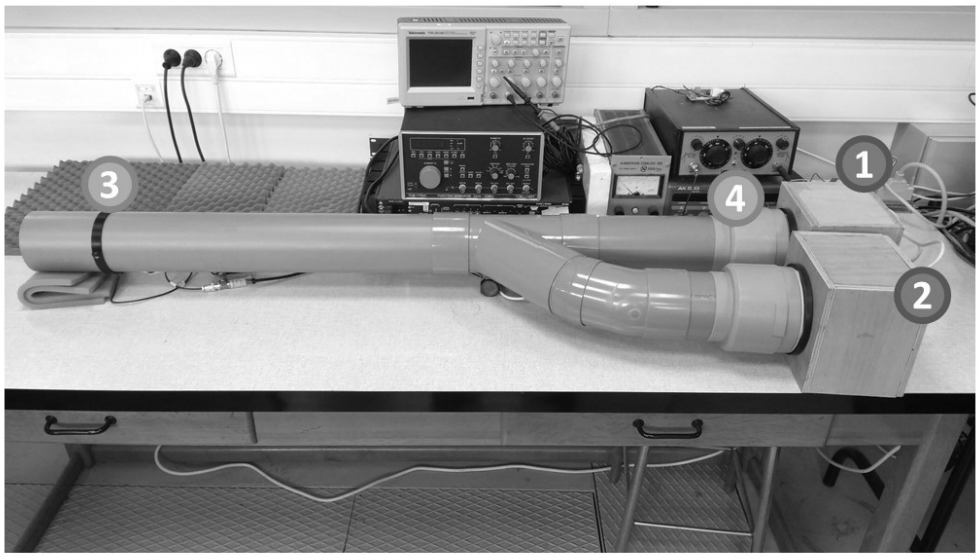

Figure 2: Duct active noise control test bench (Photo).

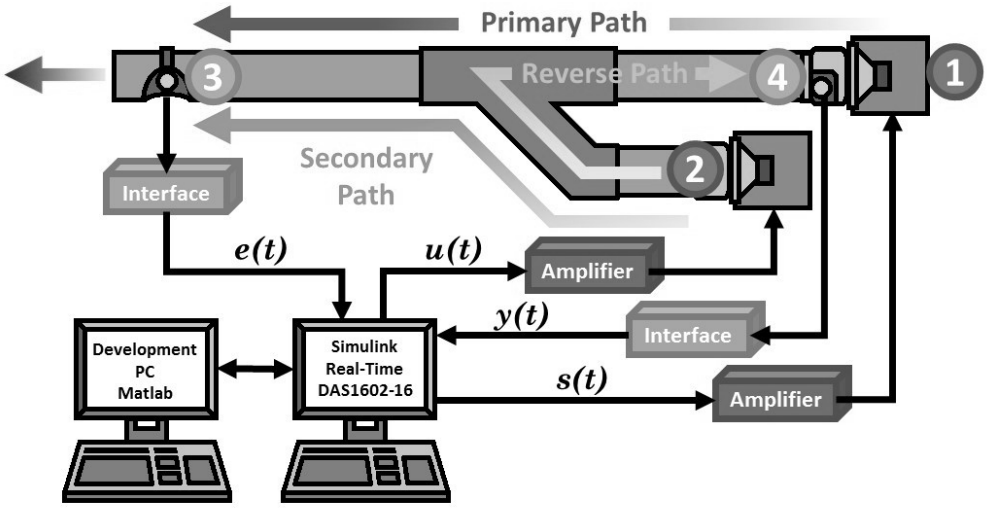

Figure 3: Duct active noise control test bench diagram.

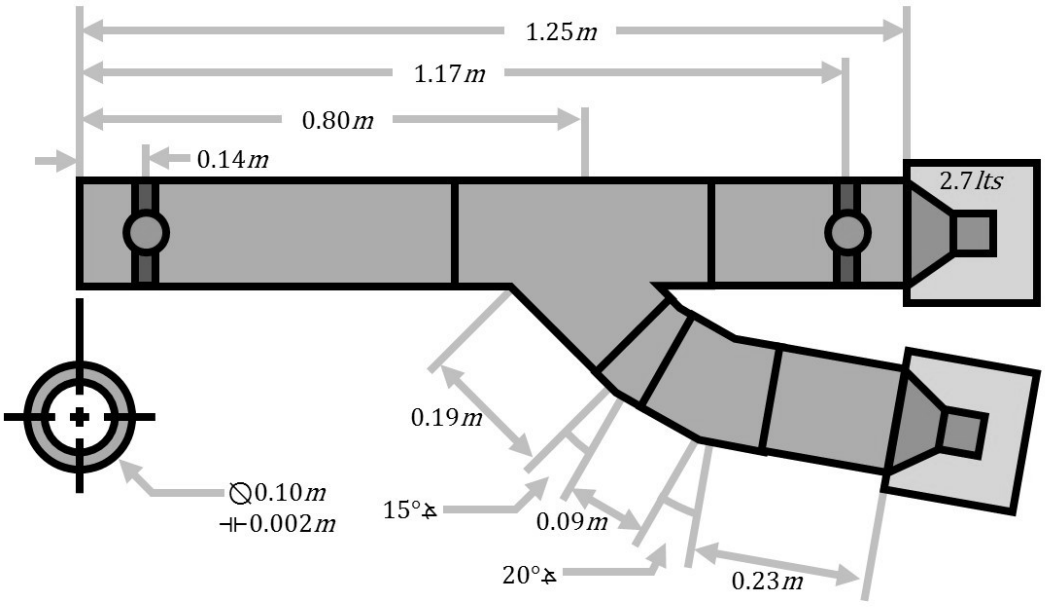

Figure 4: Duct active noise control test bench dimensions.

Both speakers are connected to a xPC Target computer with Simulink Real-time® environment through a pair of high definition power amplifiers and a data acquisition board. A second computer is used for development, design and operation with Matlab®. The sampling frequency has been chosen in accordance with the recommendations given in [8]. Taking into account that disturbances up to 400 Hz need to be attenuated, a sampling frequency $f_s = 2500$ Hz has been chosen ($T_s = 0.0004$ sec), i.e., approximately six times the maximum frequency to attenuate.

In this configuration, speakers are isolated inside wood boxes filled with special foam in order to create anechoic chambers and reduce the radiation noise produced. These boxes have dimensions $0.15\,\mathrm{m} \times 0.15\,\mathrm{m} \times 0.12\,\mathrm{m}$, giving a chamber volume of $2.7\,\mathrm{L}$.

3. System Description

The primary (T), secondary (G), and reverse (positive coupling) (M) paths are characterized by the asymptotically stable transfer operators:

$$X(q^{-1}) = q^{-d_x}\frac{B_X(q^{-1})}{A_X(q^{-1})} = q^{-d_x}\frac{b_1^X q^{-1} + \ldots + b_{n_{B_X}}^X q^{-n_{B_X}}}{1 + a_1^X q^{-1} + \ldots + a_{n_{A_X}}^X q^{-n_{A_X}}}, \tag{1}$$

with $B_X = q^{-1}B_X^*$ for any $X \in \{G, M, T\}$. $\hat{G} = q^{-d_G}\frac{\hat{B}_G}{a_G}$, $\hat{M} = q^{-d_M}\frac{\hat{B}_M}{a_M}$, and $\hat{T} = q^{-d_T}\frac{\hat{B}_T}{a_T}$ denote the identified (estimated) models of G, M, and T.

The system's order is defined by (the indexes G, M, and T have been omitted):

$$n = max(n_A, n_B + d). \tag{2}$$

The models of the systems have been identified experimentally using the identification procedure described in [9].

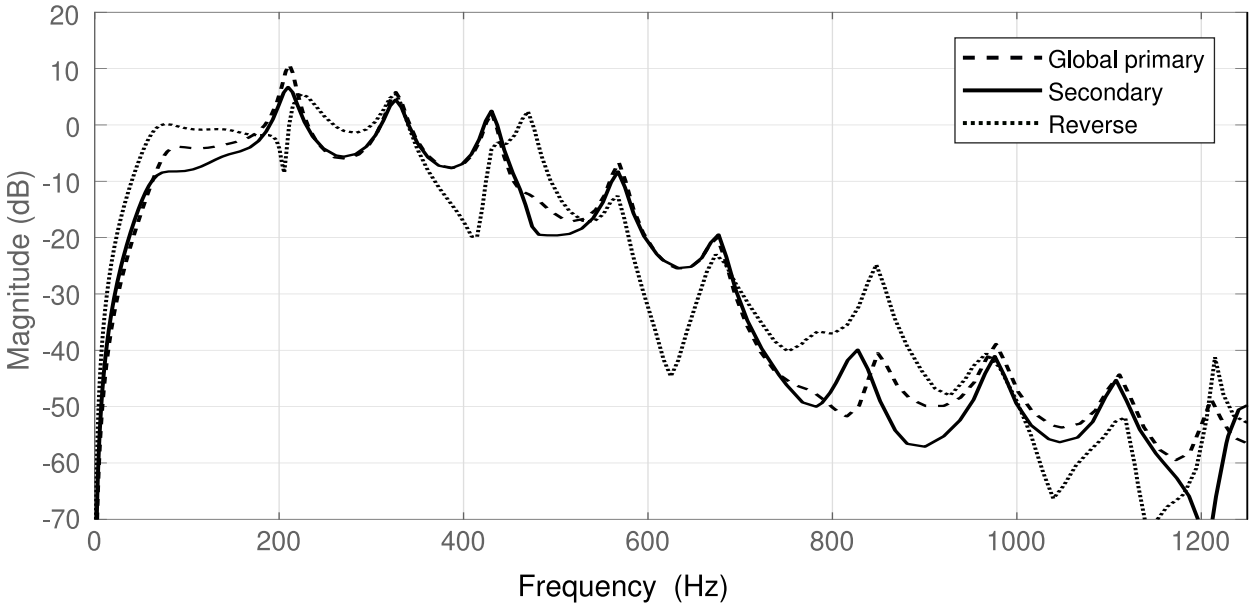

Figure 5: Frequency characteristics of the Primary, Secondary and Reverse paths identified models.

The frequency characteristics[5] of the identified models for the primary[6], secondary and reverse paths are shown in Fig. 5. These characteristics present multiple resonances (low damped complex poles) and anti-resonances (low damped complex zeros).

One can see that the secondary path has sufficient gain between 150 to 425 Hz, which means that disturbances can be efficiently attenuated in this zone. It is also clear that the reverse path has a significant gain on a large frequency range so its effect can not be neglected.

The orders and the pure delays of the various identified models are given in Table 1. One observes that the secondary path transfer operator has a pure delay of 9 sampling periods and the primary path has a pure delay of 8 sampling periods (coherent values with the length of the two paths - see Fig. 4).

Model	n_B	n_A	d
Primary	20	27	8
Secondary	20	27	9
Reverse	33	33	4

Table 1: Orders of the identified system paths.

[5]It expresses the gain of the system in the frequency domain. The gain is a non-dimensional quantity.

[6]The primary path model has been exclusively used for simulation purposes only.

4. Adaptive Infinite/Finite Impulse Response (IIR/FIR) feedforward compensators for Active Noise Control (ANC)

The corresponding block diagrams in open-loop operation and with the compensator system are shown in Fig. 6. The signal $z(t)$ is the image of the disturbance measured when the compensator system is not used (open-loop). The signal $\hat{y}(t)$ denotes the effective output provided by the measurement device when the compensator system is active and which will serve as input to the adaptive feedforward compensator $\hat{N}$. The output of this filter, denoted by $\hat{u}(t)$, is applied to the actuator through an amplifier. The transfer function G (the secondary path) characterizes the dynamics from the output of the filter $\hat{N}$ to the residual noise measurement (amplifier + actuator + dynamics of the acoustic system). The unmeasurable value of the output of the primary path (when the compensation is active) is denoted $x(t)$.

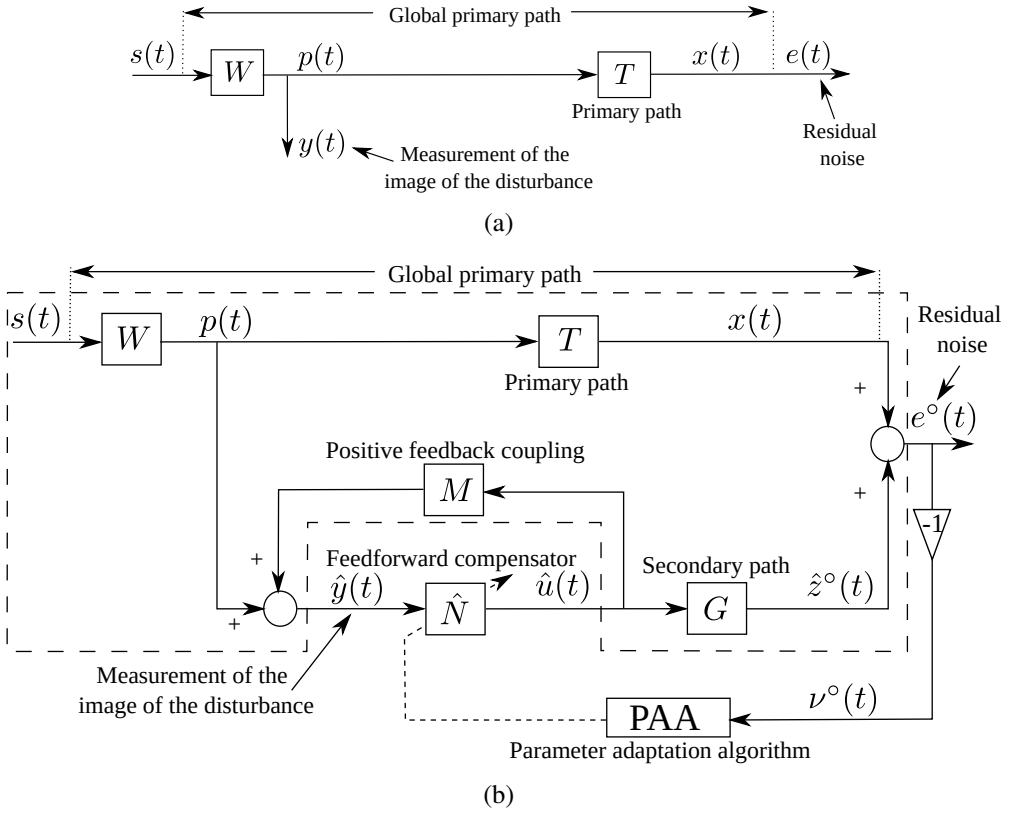

Figure 6: Feedforward active noise control (ANC): in open-loop (a) and with adaptive feedforward compensator (b).

The coupling between the output of the feedforward compensator and the measurement $\hat{y}(t)$ through the compensator actuator is denoted by M. As indicated in Fig. 6, this coupling is a "positive" feedback. The positive feedback may destabilize the system.[7] The system is no longer a pure feedforward compensator.

[7] Different solutions for reducing the effect of this internal positive feedback are reviewed in [10, 11].

The objective is to adapt the parameters of the feedforward compensator $N(q^{-1})$ such that the measured residual noise be minimized in the sense of a certain criterion while assuring the stability of the internal positive feedback loop. The optimal IIR feedforward filter (unknown) is defined by:

$$N(q^{-1}) = \frac{R(q^{-1})}{S(q^{-1})}, \tag{3}$$

where

$$R(q^{-1}) = r_0 + r_1 q^{-1} + \ldots + r_{n_R} q^{-n_R}, \tag{4}$$
$$S(q^{-1}) = 1 + s_1 q^{-1} + \ldots + s_{n_S} q^{-n_S} = 1 + q^{-1} S^*(q^{-1}). \tag{5}$$

The estimated compensator is denoted by $\hat{N}(q^{-1})$ or $\hat{N}(\hat{\mathbf{w}}, q^{-1})$ when it is a linear filter with constant coefficients or $\hat{N}(t, q^{-1})$ during estimation (adaptation) of its parameters. The optimal FIR compensator structure is obtained by taking $S = 1$ (i.e. $s_i = 0$, $\forall i = 1 : n_S$).

The input of the feedforward compensator is denoted by $\hat{y}(t)$ and it corresponds to the sum between the disturbance image in the absence of compensation and of the output of the positive feedback path. In the absence of the compensation loop (open-loop operation): $\hat{y}(t) = p(t)$. The *a posteriori*[8] output of the feedforward compensator (which is the control signal applied to the secondary path) is denoted by $\hat{u}(t+1) = \hat{u}(t+1|\hat{\mathbf{w}}(t+1))$. The input-output relationship for the estimated feedforward compensator is given by the equation of the *a posteriori* output:

$$\begin{aligned}\hat{u}(t+1) &= \hat{u}(t+1|\hat{\mathbf{w}}(t+1)) = -\hat{S}^*(t+1, q^{-1})\hat{u}(t) + \hat{R}(t+1, q^{-1})\hat{y}(t+1) \\ &= \hat{\mathbf{w}}^T(t+1)\mathbf{u}(t) = \left[\hat{\mathbf{w}}_S^T(t), \hat{\mathbf{w}}_R^T(t)\right] \begin{bmatrix} \mathbf{u}_{\hat{u}}(t) \\ \mathbf{u}_{\hat{y}}(t) \end{bmatrix},\end{aligned} \tag{6}$$

where $\hat{\mathbf{w}}$ is the estimated parameter vector and $\mathbf{u}$ is the measurement vector whose expressions are given below:

$$\hat{\mathbf{w}}^T(t) = [\hat{s}_1(t), \ldots \hat{s}_{n_S}(t), \hat{r}_0(t), \ldots \hat{r}_{n_R}(t)] = [\hat{\mathbf{w}}_S^T(t), \hat{\mathbf{w}}_R^T(t)], \tag{7}$$
$$\begin{aligned}\mathbf{u}^T(t) &= [-\hat{u}(t), -\hat{u}(t-n_S+1), \hat{y}(t+1), \ldots \hat{y}(t-n_R+1)] \\ &= [\mathbf{u}_{\hat{u}}^T(t), \mathbf{u}_{\hat{y}}^T(t)],\end{aligned} \tag{8}$$

and $\hat{u}(t)$, $\hat{u}(t-1)$, ... are the *a posteriori* outputs of the feedforward compensator generated by

$$\hat{u}(t) = \hat{u}(t|\hat{\mathbf{w}}(t)) = \hat{\mathbf{w}}^T(t)\mathbf{u}(t-1), \tag{9}$$

while $\hat{y}(t+1)$, $\hat{y}(t)$, ... are the measurements provided by the primary transducer.[9]

The measured residual error satisfies the following equation:

$$e^\circ(t+1) = x(t+1) + \hat{z}^\circ(t+1). \tag{10}$$

[8] In adaptive control and estimation the predicted output at t can be computed either on the basis of the previous parameter estimates (*a priori*) or on the basis of the current parameter estimates (*a posteriori*).

[9] $\hat{y}(t+1)$ is available before adaptation of parameters starts at $t+1$.

The *a priori* adaptation error is defined as

$$\nu^{\circ}(t+1) = -e^{\circ}(t+1) = -x(t+1) - \hat{z}^{\circ}(t+1). \tag{11}$$

The development or analysis of the PAA for estimating in real-time the parameter vector $\hat{\mathbf{w}}$ assumes that

- (Perfect matching condition) There exists a value of the feedforward filter parameters such that[10]
$$\frac{N}{(1-NM)}G = -T \tag{12}$$
- and the characteristic polynomial of the "internal" feedback loop:
$$P(z^{-1}) = A_M(z^{-1})S(z^{-1}) - B_M(z^{-1})R(z^{-1}) \tag{13}$$
is a Hurwitz polynomial.

So the objective of the adaptation algorithm will be to allow the compensator $\hat{N}$ to approach the optimal value at least in the frequency range of interest.

Nevertheless, in the context of the present paper these hypothesis are violated. What it is expected is that the minimization of the residual error in a frequency band will lead to a stable internal loop.

The various FIR/IIR adaptive compensation algorithm which have been tested are summarized in Table 2. All the algorithms can be characterized by the use of a particular form of the parameter adaptation algorithm (PAA) which will be presented next and of a specific "regressor vector" (observation vector) generated through the filtering of available measurements.

4.1. Parameter Adaptation Algorithm (PAA)

Based on stability considerations, a general form for the PAAs has been proposed in [12] which can be expressed using the formalism of [13] as:

$$\mathbf{r}(t) = \mathbf{u}_f(t) = L(q^{-1})\mathbf{u}(t) \tag{14}$$

$$\mathbf{k}(t) = \frac{\mathbf{F}(t)\mathbf{r}(t)}{1+\mathbf{r}(t)^T\mathbf{F}(t)\mathbf{r}(t)} \tag{15}$$

$$\hat{\mathbf{w}}(t+1) = \hat{\mathbf{w}}(t) + \mathbf{k}(t)\nu^{\circ}(t+1) \tag{16}$$

$$\nu(t+1) = \frac{\nu^{\circ}(t+1)}{1+\mathbf{r}^T(t)\mathbf{F}(t)\mathbf{r}(t)} \tag{17}$$

$$\mathbf{F}(t+1) = \frac{1}{\lambda_1(t)}\left[\mathbf{F}(t) - \frac{\mathbf{F}(t)\mathbf{r}(t)\mathbf{r}^T(t)\mathbf{F}(t)}{\frac{\lambda_1(t)}{\lambda_2(t)} + \mathbf{r}(t)^T(t)\mathbf{F}(t)\mathbf{r}(t)}\right] \tag{18}$$

$$1 \geq \lambda_1(t) > 0 \quad ; \quad 0 \leq \lambda_2(t) < 2 \quad ; \quad F(0) > 0 \tag{19}$$

$\lambda_1(t)$ and $\lambda_2(t)$ allow to obtain various profiles for the adaptation gain matrix $\mathbf{F}(t)$. Four cases are of interest:

[10]The parenthesis (q^{-1}) or (z^{-1}) will be omitted in some of the following equations to make them more compact.

- Constant trace algorithm. $\lambda_1(t)$ and $\lambda_2(t)$ are adjusted continuously to maintain constant the trace of the adaptation gain matrix. This allows to move in the optimal direction of the least squares while maintaining the adaptation capabilities. Nevertheless, for accelerating the adaptation transient it may be useful to use a larger adaptation gain transiently.

- Decreasing adaptation gain ($\lambda_1 = 1$, $\lambda_2 = 1$). This is used in self-tuning regime and for initialization of the constant trace algorithm with a higher gain as well as for self-tuning operation (convergence towards a fixed feedforward compensator).

- Variable forgetting factor. This option can be also used for initialization of the constant trace algorithm. The difference is that in this option $\lambda_1(0) < 1$ but it will tend asymptotically to 1. This allows to get transiently a higher adaptation gain than the one used in the constant trace algorithm [12].

- Constant scalar adaptation gain. This is obtained by taking $\mathbf{F}(t) = \gamma\mathbf{I}$, where $\mathbf{I}$ is the identity matrix. One gets a scalar adaptation gain. In this case **k(t)** is given by:

$$\mathbf{k}(t) = \frac{\gamma\mathbf{r}(t)}{1+\gamma\mathbf{r}^T\mathbf{r}(t)} \tag{20}$$

In order to maintain constant the trace of the adaptation gain matrix the values of $\lambda_1(t)$ and $\lambda_2(t)$ are determined from the equation:

$$tr\left(\mathbf{F}(t+1)\right) = \frac{1}{\lambda_1(t)} tr\left(\mathbf{F}(t) - \frac{\mathbf{F}(t)\mathbf{r}(t)\mathbf{r}^T(t)\mathbf{F}(t)}{\alpha(t)+\mathbf{r}^T(t)\mathbf{F}(t)\mathbf{r}(t)}\right) \tag{21}$$

fixing the ratio $\alpha(t) = \lambda_1(t)/\lambda_2(t)$.

The updating of matrix $\mathbf{F}(t)$ is done using the U-D factorization for numerical robustness reason. The details of this algorithm can be found in [8, 12].[11]

When using a scalar adaptation gain, one can see that for very small values of γ one can approximate Eq. (20) by $\mathbf{k}(t) = \gamma\mathbf{r}(t)$ and therefore Eq. (16) by

$$\hat{\mathbf{w}}(t+1) = \hat{\mathbf{w}}(t) + \gamma\mathbf{r}v^\circ(t+1), \tag{22}$$

which corresponds almost to the adaptation algorithm used in Filtered u least mean square (FULMS) for IIR compensators [14] and to the filtered x least mean squares (FXLMS) for FIR compensators[15] algorithms except that since the adaptation gain is small and the residual error will vary slowly the quantity $\mathbf{r}(t)v^\circ(t+1)$ is replaced by $\mathbf{r}(t-1)v^\circ(t)$.

In Table 2, column 1 gives the adaptation algorithms using a matrix adaptation gain derived from stability considerations: Filtered u pseudo linear regression (FUPLR) and Filtered u stability based (FUSBA). Column 2 gives the adaptation algorithms using scalar adaptation gain also derived from stability considerations: normalized filtered u least mean squares (NFULMS) and

[11] Routines for the implementation of the algorithm can be downloaded from `http://www.gipsa-lab.grenoble-inp.fr/~ioandore.landau/adaptivecontrol/`

	Paper (Matrix gain)	Paper (Scalar gain)	FULMS (FXLMS) (Scalar gain)
$\hat{\mathbf{w}}(t+1) =$	$\hat{\mathbf{w}}(t)+F(t)\mathbf{r}(t)\frac{v^\circ(t+1)}{1+\mathbf{r}^T(t)F(t)\mathbf{r}(t)}$	$\hat{\mathbf{w}}(t)+\gamma(t)\mathbf{r}(t)\frac{v^\circ(t+1)}{1+\gamma(t)\mathbf{r}^T(t)\mathbf{r}(t)}$	$\hat{\mathbf{w}}(t)+\gamma(t)\mathbf{r}(t-1)v^\circ(t)$
Adapt. gain	$F(t+1)^{-1}=\lambda_1(t)F(t)+$ $+\lambda_2(t)\mathbf{r}(t)\mathbf{r}^T(t)$ $0\le\lambda_1(t)<1, 0\le\lambda_2(t)<2$ $F(0)>0$	$\gamma(t)>0$	$\gamma(t)>0$
Adaptive	Decr. gain and const. trace	$\gamma(t)=\gamma=const$	$\gamma(t)=\gamma=const$
Self tuning	$\lambda_2=const.$ $\lim_{t\to\infty}\lambda_1(t)=1$	$\sum_{t=1}^{\infty}\gamma(t)=\infty, \quad \lim_{t\to\infty}\gamma(t)=0$	$\sum_{t=1}^{\infty}\gamma(t)=\infty, \quad \lim_{t\to\infty}\gamma(t)=0$
$\mathbf{u}^T(t) =$	$[-\hat{y}(t),\ldots,\hat{u}(t+1),\ldots]$	$[-\hat{y}(t),\ldots,\hat{u}(t+1),\ldots]$	$[-\hat{y}(t),\ldots,\hat{u}(t+1),\ldots]$
$\mathbf{r}(t) =$	$L\mathbf{u}(t)$ FUPLR: $L=\hat{G}$ FUSBA: $L=\frac{a_M}{\hat{P}}\hat{G}$ $\hat{P}=a_M\hat{S}-\hat{B}_M\hat{R}$	$L\mathbf{u}(t)$ NFULMS: $L=\hat{G}$ SFUSBA: $L=\frac{a_M}{\hat{P}}\hat{G}$ $\hat{P}=a_M\hat{S}-\hat{B}_M\hat{R}$	$L\mathbf{u}(t)$ $L=\hat{G}$
$M=\frac{B_M}{A_M}$	$B_M=b_{1_M}z^{-1}+b_{2_M}z^{-2}+\ldots$		
	$A_M=1+a_{1_M}z^{-1}+a_{2_M}z^{-2}+\ldots$		$A_M=1$
Stability condition	$\frac{A_MG}{PL}-\frac{\lambda}{2}=SPR$ $\lambda=\max\lambda_2(t)$	$\frac{A_MG}{PL}=SPR$	Unknown

Table 2: Algorithms for IIR (FIR) adaptive feedforward compensation in active noise control (ANC) with acoustic coupling.

scalrar filtered u stability based (SFUSBA). Column 3 gives the now classical FULMS algorithm which uses a scalar adaptation gain (and which corresponds to the FXLMS algorithm when using an FIR compensator). The connections with the NFULMS have been enhanced above. An important observation is that the compensator can be implemented as a FIR or an IIR filter.

The last row of Table 2 summarizes the stability conditions in a deterministic context (asymptotic stability condition for any initial condition on the parameters of the IIR/FIR compensator assuming that a perfect matching solution exist). Despite the fact that the basic hypotheses for stability analysis are violated, it was observed that these "strictly positive real" (SPR) conditions play a fundamental role even in the present context. The reason is that these SPR conditions can be interpreted as approximation conditions with respect to the true gradient [16], namely the approximated gradient used should be within an angle of $\pm 90^\circ$ with respect to the true gradient.

A key role in the various adaptation algorithms is played by the filter L, that helps to satisfy the "strictly positive real condition".

The following procedure is used at each sampling time for implementing the adaptive feedforward compensation:

1. Get the measured image of the disturbance $\hat{y}(t+1)$, the measured residual error $e^\circ(t+1)$, and compute $v^\circ(t+1)=-e^\circ(t+1)$.

2. Compute $\mathbf{u}(t)$ and $\mathbf{r}(t)$ using Eqs (8) and (14).
3. Estimate the parameter vector $\hat{\mathbf{w}}(t+1)$ using the PAA given in Eqs (17)-(16).
4. Compute and apply the control $\hat{u}(t+1)$ given in Eq. (6).

5. Youla–Kučera Parametrized Adaptive Feedforward Compensators

The rationale behind the use of the Youla–Kučera parametrized feedforward compensator is to separate the problem of the stabilization of the positive internal loop from the problem of the minimization of the residual noise [5]. In order to achieve this, instead of a standard FIR or IIR feedforward compensator, one can use an Youla–Kučera parametrization of the adaptive feedforward compensator. The central compensator will assure the stability of the internal positive feedback loop and its performance are enhanced in real-time by the direct adaptation of the parameters of the Youla–Kučera Q filter.

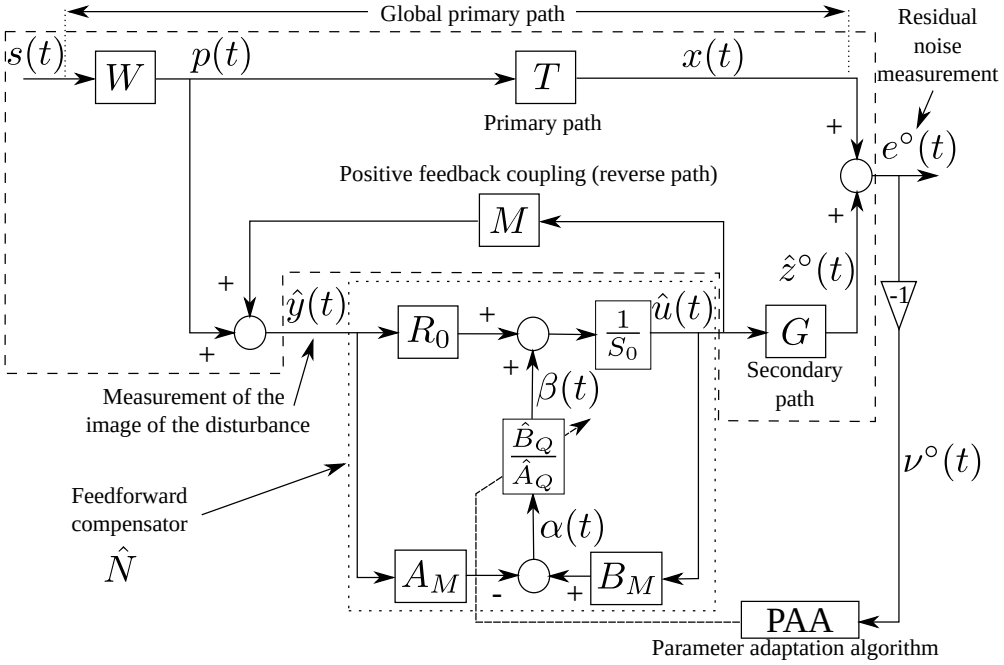

Figure 7: Adaptive feedforward disturbance compensation using Youla–Kučera parametrization.

A block diagram of such an adaptive feedforward compensator is shown in Fig. 7. FIR and IIR Q filters can be used. Details of the specific algorithms can be found in [3, 16]. The transfer operators of the various paths of the ANC system have been given in Section 3.

The optimal Youla–Kučera IIR (YKIIR) feedforward compensator which will minimize the residual noise can be written, using this parametrization, as:

$$N(q^{-1}) = \frac{R(q^{-1})}{S(q^{-1})} = \frac{A_Q(q^{-1})R_0(q^{-1}) - B_Q(q^{-1})A_M(q^{-1})}{A_Q(q^{-1})S_0(q^{-1}) - B_Q(q^{-1})B_M(q^{-1})} \tag{23}$$

where the optimal Youla–Kučera filter $Q(q^{-1})$ can have an IIR or a FIR structure:

$$Q(q^{-1}) = \frac{B_Q(q^{-1})}{A_Q(q^{-1})} = \frac{b_0^Q + b_1^Q q^{-1} + \ldots + b_{n_{B_Q}}^Q q^{-n_{B_Q}}}{1 + a_1^Q q^{-1} + \ldots + a_{n_{A_Q}}^Q q^{-n_{A_Q}}} \tag{24}$$

$R_0(q^{-1})$, $S_0(q^{-1}) = 1 + q^{-1}S_0^*(q^{-1})$ are the polynomials of the central (stabilizing) filter and $A_M(q^{-1})$, $B_M(q^{-1})$ are given in Eq. (1). The FIR Q filter corresponds to $A_Q = 1$, i.e. $a_i^Q = 0$ for $i = 1$ to n_{A_Q}.

An equivalent representation for the YK feedforward compensator is shown in Figure 8. This equivalent representation allows to enhance the fact that for the particular case $R_0 = 0$ the YK feedforward compensator contains implicitly a "neutralization filter" in order to compensate the internal positive feedback present in the system.

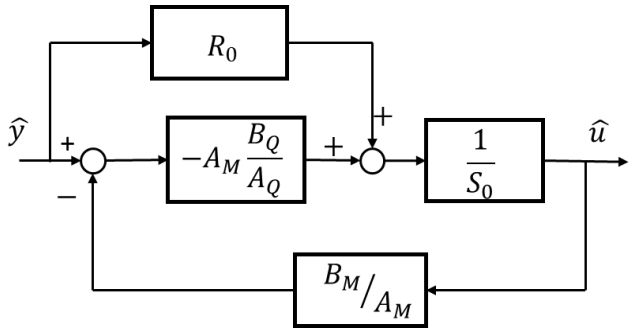

Figure 8: Equivalent representation of the Youla Kučera compensator.

Details on YK algorithms for adaptive feedforward compensation can be found in [2],[16]. Table 3 summarizes the YK type adaptation algorithms used in the various cases as well as the structure of the filters introduced for stability reasons. We will focus next on the YKFIR algorithm which is the algorithm assuring a stable operation in the context of a delay of the secondary path larger than the delay of the primary path.

5.1. Youla–Kučera Finite Impulse Response (YKFIR) Filter

Let's begin by considering Youla–Kučera FIR filters, for which $A_Q(q^{-1}) = 1$. The estimated YKFIR filter is denoted by $\hat{Q}(q^{-1})$ or $\hat{Q}(\hat{\mathbf{w}}, q^{-1})$ when it is a linear filter with constant coefficients or $\hat{Q}(t, q^{-1})$ during estimation (adaptation). The vector of parameters for the estimated $\hat{Q}$ filter

$$\hat{Q}(q^{-1}) = \frac{\hat{B}_Q(q^{-1})}{1} = \hat{b}_0^Q + \hat{b}_1^Q q^{-1} + \ldots + \hat{b}_{n_{B_Q}}^Q q^{-n_{B_Q}} \tag{25}$$

is denoted by

$$\hat{\mathbf{w}}^T = [\hat{b}_0^Q, \ldots, \hat{b}_{n_{B_Q}}^Q] = \hat{\mathbf{w}}_{B_Q}^T. \tag{26}$$

The PAAs have been developed from a stability point of view assuming that:

- (Perfect matching condition) There exists a value of the Q filter parameters such that

$$\frac{G \cdot A_M(R_0 - A_M B_Q)}{A_M S_0 - B_M R_0} = -D \tag{27}$$

- There exists a central feedforward compensator N_0 (R_0, S_0) which stabilizes the internal positive feedback loop formed by N_0 and M and the characteristic polynomial of the closed-loop

$$P_0(z^{-1}) = A_M(z^{-1})S_0(z^{-1}) - B_M(z^{-1})R_0(z^{-1}) \tag{28}$$

is a Hurwitz polynomial[12].

What it is important to underline, is that in the context of this paper while the first hypothesis is violated, the second is definitely true since the central controller is designed such that the poles of the internal closed loop be asymptotically stable (These poles remain constant independently of the values of the parameters of the FIR Q filter[13]). This is a fundamental difference with respect to the case of using a standard FIR adaptive compensator (see Section 4).
The control signal for the YKFIR is expressed as:

$$\hat{u}(t+1) = \hat{u}(t+1|\hat{\mathbf{w}}(t+1)) = -S_0^*(q^{-1})\hat{u}(t) + R_0(q^{-1})\hat{y}(t+1) + \hat{\mathbf{w}}^T(t+1)\mathbf{u}(t) \tag{29}$$

where $\hat{\mathbf{w}}(t)$ and $\mathbf{u}(t)$ are given in Table 3. The PAAs are exactly of the same structure as those given in Eqs (14)-(18). All the considerations regarding the type of adaptation gain and its profile remain valid. In order to satisfy the positive real condition for stability, the introduction of the filter L on the measured quantities is important.

Several choices for the filter L will be considered, leading to different algorithms (see Table 3):

FUPLR and NFULMS: $L = \hat{G}$

FUSBA and SFUSBA: $L = \frac{a_M}{\hat{P}_0}\hat{G}$ with $\hat{P}_0 = a_M S_0 - \hat{B}_M R_0$

The major difference with respect to the standard IIR or FIR compensators as well as with respect to YKIIR compensators is that the FUSBA algorithm can be implemented from the beginning since the polynomial $\hat{P}_0$ is known and remains unchanged during the adaptation process (for YKIIR the filter to be used will depend on currently estimated parameters). This is a significant advantage and this is the key point for assuring a stable operation when the delay of the secondary path is larger than the delay of the primary path.

[12] For $R_0 = 0$ and $S_0 = 1$ one has $P_0 = A_M$

[13] Connecting in positive feedback the YK compensator given in Eq. (23) for $A_Q = 1$ with the reverse path $M = \frac{B_M}{A_M}$, it can be verified by simple calculations that the closed loop poles of the internal loop are given by Eq. (28) independently of the values of the Q filter.

	YKIIR	YKFIR	YKIIR	YKFIR
	Matrix adaptation gain		Scalar adaptation gain	
$\hat{\mathbf{w}}(t+1) =$	$\hat{\mathbf{w}}(t) + F(t)\mathbf{r}(t)\frac{v^{\circ}(t+1)}{1+\mathbf{r}^T(t)F(t)\mathbf{r}(t)}$		$\hat{\mathbf{w}}(t) + \gamma(t)\mathbf{r}(t)\frac{v^{\circ}(t+1)}{1+\gamma(t)\mathbf{r}^T(t)\mathbf{r}(t)}$	
Adapt. gain	$F(t+1)^{-1} = \lambda_1(t)F(t) + \lambda_2(t)\mathbf{r}(t)\mathbf{r}^T(t)$ $0 \le \lambda_1(t) < 1,\ 0 \le \lambda_2(t) < 2,\ F(0) > 0$		$\gamma(t) > 0$	
Adaptive	Decr. gain and const. trace		$\gamma(t) = \gamma = const$	
Self tuning	$\lambda_2 = const.,\quad \lim_{t\to\infty} \lambda_1(t) = 1$		$\sum_{t=1}^{\infty} \gamma(t) = \infty,\quad \lim_{t\to\infty} \gamma(t) = 0$	
$\hat{\mathbf{w}}(t) =$	$[\hat{b}_0^Q, \ldots, a_1^Q, \ldots]$	$[\hat{b}_0^Q, \ldots]$	$[\hat{b}_0^Q, \ldots, a_1^Q, \ldots]$	$[\hat{b}_0^Q, \ldots]$
$\mathbf{u}^T(t) =$	$[\alpha(t+1), \ldots, \beta(t), \ldots]$ $\alpha(t) = B_M\hat{u}(t) - A_M\hat{y}(t)$ $\beta(t) = S_0\hat{u}(t) - R_0\hat{y}(t)$	$[\alpha(t+1), \ldots]$ $\alpha(t) = B_M\hat{u}(t)$ $-A_M\hat{y}(t)$	$[\alpha(t+1), \ldots, \beta(t), \ldots]$ $\alpha(t) = B_M\hat{u}(t) - A_M\hat{y}(t)$ $\beta(t) = S_0\hat{u}(t) - R_0\hat{y}(t)$	$[\alpha(t+1), \ldots]$ $\alpha(t) = B_M\hat{u}(t)$ $-A_M\hat{y}(t)$
$\hat{P} =$	$a_Q(a_M S_0 - \hat{B}_M R_0)$	$a_M S_0 - \hat{B}_M R_0$	$a_Q(a_M S_0 - \hat{B}_M R_0)$	$a_M S_0 - \hat{B}_M R_0$
$P =$	$A_Q(A_M S_0 - B_M R_0)$	$A_M S_0 - B_M R_0$	$A_Q(A_M S_0 - B_M R_0)$	$A_M S_0 - B_M R_0$
$\mathbf{r}(t) =$	$L\mathbf{u}(t)$ FUPLR: $L = \hat{G}$ FUSBA: $L = \frac{a_M}{\hat{P}}\hat{G}$		$L\mathbf{u}(t)$ NFULMS: $L = \hat{G}$ SFUSBA: $L = \frac{a_M}{\hat{P}}\hat{G}$	
Stability condition	$\frac{A_M G}{PL} - \frac{\lambda}{2} = SPR \quad (\lambda = \max \lambda_2(t))$		$\frac{A_M G}{PL} = SPR$	

Table 3: Algorithms for Youla–Kučera parametrized adaptive feedforward compensation in ANC with acoustic coupling.

5.2. Design of the Central Controller

The main objective of the central controller $N_0(q^{-1}) = \frac{R_0(q^{-1})}{S_0(q^{-1})}$ is to guarantee the stability of the internal positive feedback loop. This can be achieved by using a pole placement design technique (see also [8, Chapter 7]) taking into account that the feedback is positive. All stable poles of the reverse path can be assigned as poles of the closed loop. In order to obtain a small attenuation of the high amplitude picks, one can modify the damping of the poles at the frequencies of those picks. Additional stable poles can be assigned and some fixed part can be added in order to reach some specifications (opening of the loop at 0 Hz and at $0.5 f_S$, reducing the maximum of the disturbance–residual noise sensitivity function, etc.). A very interesting particular case which drastically simplify the implementation is to choose the desired poles of the internal closed loop as $P_0 = A_M$. This can be achieved by taking $S_0 = 1$ ($S_0^* = 0$) and $R_0 = 0$. Not only the central controller is drastically simplified but the FUPLR and FUSBA algorithms become identical and therefore the filter L is simpler (simulation results for this algorithm are presented in Appendix B.

5.3. Youla–Kučera Parametrization—Some Remarks

Two major observations when using the Youla–Kučera parametrization have to be made:

- If an FIR Q filter is used, the poles of the internal closed loop will be defined by the central compensator R_0, S_0 and they will remain unchanged independently of the values of the parameters of the Q filter.

- If an IIR Q filter is used, the poles of the internal closed loop will be defined by the central controller but additional poles corresponding to the denominator of the estimated Q filter will be added. When the delay of the secondary path is larger than the delay of the primary path, it was observed that the denominator of the estimated Q filter becomes unstable. The use of lattice form algorithms [17], [18] may be an issue in order to force the denominator of the IIR Q filter to remain stable.

As for the standard IIR (FIR) feedforward adaptive compensators described in Section 4, scalar adaptation gains can also be used.
The implementation procedure is similar to that for the FIR compensators except that $\hat{\mathbf{w}}(t)$ and $\mathbf{r}(t)$ are given in Table 3, and the control $u(t+1)$ is given in Eq. (29).

6. Simulation Results

The objective of this section is to assess comparatively the performance of the various adaptive feedforward compensation schemes for attenuating broad-band noise disturbances with unknown and time-varying characteristics. All the algorithms mentioned in Tables 3 and 4 have been tested, but only the FIR FUSBA and the YKFIR algorithms have assured a stable operation of the test bench and of the simulations. Decreasing of the adaption gain only pushes forward in time the instability phenomenon. As a consequence only the FIR FUSBA and the YKFIR FUSBA will be further evaluated in terms of performance.

6.1. Number of Adjustable Parameters

The performance of the various compensators will depend on the number of parameters. For a selected PAA various complexities of the feedforward compensator have been tested. A compromise between performance/complexity has to be considered and this value is used for further investigation.

6.2. Type of Parameter Adaptation Algorithms

For a given complexity of the feedforward compensator (60 parameters) the performance obtained with various PAAs have been evaluated. The attenuation is measured on a sample of 3s as the ratio between the variance of the residual noise in the absence of the compensator and the variance of the residual noise in the presence of the compensator. The obtained result is then transformed into decibels.

6.3. Description of Simulations and Results

In this section, simulation results for the Youla-Kučera FIR and the standard FIR feedforward compensators are presented. The disturbance signal used in these simulations is a pseudo random binary sequence (PRBS) generated by a register with $N = 15$ cells passed through a band-pass filter with cut-off frequencies at 150 Hz and 350 Hz. To make these simulation closer to the

Filter type	No. params. [num/den]	Attenuation (dB)
YKFIR	20/0	13.28
YKFIR	30/0	14.55
YKFIR	40/0	19.25
YKFIR	50/0	19.53
YKFIR	60/0	21.02
YKFIR	70/0	21.82
YKFIR	80/0	22.01

Table 4: Influence of the number of parameters on the performance of the YKFIR adaptive compensator (150-350 Hz broad-band disturbance, decreasing gain, 180 sec, simulation).

experimental case, we have introduced small changes in the poles and zeros of the reverse and secondary path models used for the simulation of the system by making these closer to the unit circle (as such there will be a difference between the values of the identified model parameters used in the filters and the values of the parameters used in the simulator).

Filter type	No. params. [num/den]	Adaptation algorithm	Att. (dB)
YKFIR	60/0	NFULMS (scalar gain)	unstable
YKFIR	60/0	FUPLR (matrix gain)	unstable
YKFIR	60/0	SFUSBA (scalar gain)	15.23
YKFIR	60/0	FUSBA (matrix gain)	21.02

Table 5: Influence of the adaptation algorithm on the performance of YKFIR adaptive compensators (150-350 Hz broad-band disturbance, decreasing gain, 180 sec, simulation).

Table 4 summarizes the obtained attenuation results for the YKFIR adaptive filter for various filter orders and the FUSBA adaptation algorithm with decreasing gain. The initial gain is chosen to be of 0.1 per parameter, which implies an initial trace of the adaptation matrix of 0.1 times the number of adapted parameters. The simulation is done over a time duration of 180 sec, where the control algorithm is activated after 15 sec. From these results, it seems that the $60/0$ filter order is a good compromise in terms of attenuation vs. complexity. For the rest of these simulation results, the $60/0$ order filter will be used.

Table 5 shows a comparison of various adaptation algorithms for the $60/0$ YKFIR feedforward filter. For the scalar gain adaptation, an initial gain of 0.02 is used. Decreasing gain adaptation is obtained by dividing the initial gain by $(1+\frac{t}{10})$, where the variable t represents the time in seconds since the beginning of the adaptation. The instability of the FUPLR and NFULMS alorithms is the consequence of the violation of the SPR condition over a large frequency range.

For the standard FIR adaptive algorithm, Table 6 shows the influence of the number of parameters on the obtained attenuation. These simulations results have been obtained by closing the loop first at 15 sec using the FUPLR algorithm and then switching to the FUSBA algorithm at 50 sec. The total simulation duration is of 180 sec. The decreasing gain algorithm is used to adapt the

Filter type	No. params. [num/den]	Attenuation (dB)
FIR	20/0	6.66
FIR	30/0	7.67
FIR	40/0	8.16
FIR	50/0	8.33
FIR	60/0	8.37
FIR	70/0	8.43
FIR	80/0	8.51

Table 6: Influence of the number of parameters on the performance of the FIR adaptive compensator (150-350 Hz broad-band disturbance, decreasing gain, 180 sec, simulation).

parameters with an initial gain of 0.01 per parameter. As for the YKFIR adaptive compensator, the disturbance's spectrum is between 150 and 350 Hz. An adaptive FIR compensator with 60 parameters has been considered for further evaluation.

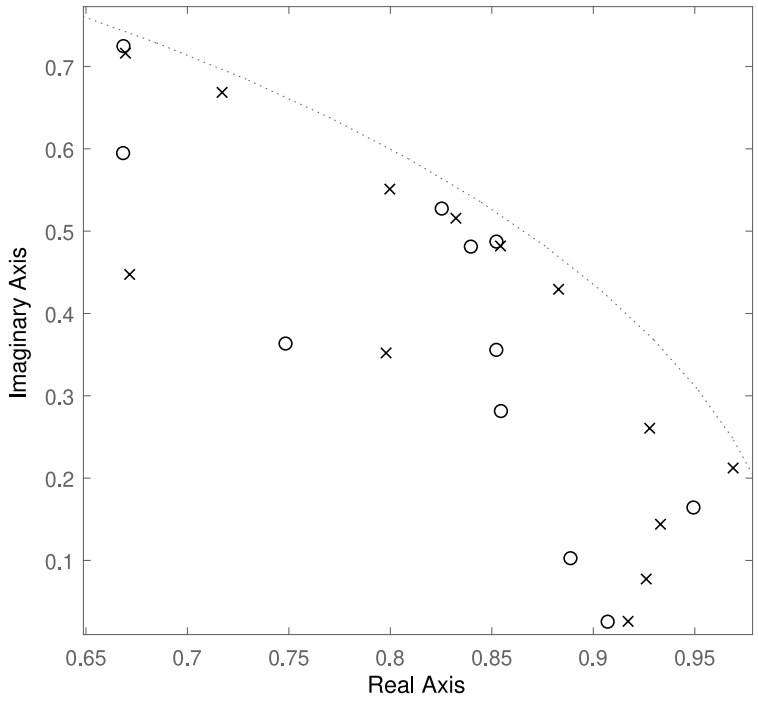

Figure 9: Zoom for the comparison of the positive feedback loop poles when using YKFIR (∘) and FIR (×) adaptive compensators (simulation).

Figure 9 can be used to compare the poles of the positive feedback loop when using the adaptive YKFIR and the adaptive FIR compensators (it is a zoom of the poles map showing the 1/4 of the map). For the standard FIR there is a pair of poles in low frequencies which are very close to the unit circle.

7. Experimental Results

The objective of this section is to compare experimentally on the test bench described in Section 2 the algorithms that showed stable results in simulation.

7.1. Protocols used for performance evaluation

In defining the experimental protocols, a number of performance indicators have to be taken into account:

- Definition of the testing signals
- Number of parameters to be adapted
- Type of PAA used
- Duration of the experiment

7.2. Testing Signals

The following type of disturbances have been considered

- broad-band noise with a flat DSP between 150 to 200 Hz, 225 to 275 Hz, 300 to 350 Hz,150 to 250 Hz, 250 to 350 Hz, 150 to 350 Hz and 150 to 350 Hz.
- PRBS noise with a flat DSP from 80 to 1250 Hz
- step change from a broad-band disturbance 150 -250 Hz to a broad-band disturbance 250 -350 Hz

A test horizon of 180 s has been chosen as a compromise between the time required to achieve many of the experiments and the convergence horizon. Few tests have been carried on a larger horizon showing the expected improvement in performance.

An important issue is the adaptation capabilities in the presence of step changes in the disturbance characteristics. The step changes occur at 180 sec.

7.3. Experimental Results for Adaptive Youla-Kučera FIR Feedforward Compensators

Filter type	No. params. [num/den]	Attenuation (dB)
YKFIR	40/0	19.79
YKFIR	60/0	20.58
YKFIR	80/0	20.66

Table 7: Influence of the number of parameters on the performance of the YKFIR (150-350 Hz broad-band disturbance, 180 s experimental).

Table 7 gives results obtained with YKFIR FUSBA for various complexities of the Q FIR filter on a 180 s experiment using a broad-band disturbance 150-350 Hz and a decreasing matrix

adaptation gain. The Q FIR filter with 60 parameters has been selected for further investigation. Table 8 gives the performance of the 60 parameters YKFIR for various PAAs and a duration of 180 s for the experiment. It can be seen that the FUSBA (matrix adaptation gain) and the SFUSBA (scalar adaptation gain) algorithms give the best results[14].

Filter type	No. params. [num/den]	Adaptation algorithm	Att. (dB)
YKFIR	60/0	NFULMS (scalar gain)	5.57
YKFIR	60/0	FUPLR (matrix gain)	5.65
YKFIR	60/0	SFUSBA (scalar gain)	19.90
YKFIR	60/0	FUSBA (matrix gain)	20.94

Table 8: Influence of the adaptation algorithm on the performance of YKFIR adaptive compensators, 180 sec, experimental.

Figure 10 gives the time-domain performance of the YKFIR configuration with 60 parameters using the FUSBA algorithm. A constant trace adaptation gain has been used with a trace of $trace = 60 \times 0.002$. The system operates in open loop for 15 s. The attenuation is evaluated every 15 secs on a horizon of 15s. One can say that the system almost reaches final attenuation after 700 s. Table 9 gives information about the transient behaviour. One can see that after 180 s almost 90% of the final performance is achieved.

Filter type	No. params. [num/den]	Duration	Attenuation (dB)
YKFIR	60/0	180s	20.58
YKFIR	60/0	800s	22.76

Table 9: Influence of the experiment's length on the performance (150-350 Hz broad-band disturbance).

Table 10 gives the performance of the YKFIR for various types of broad-band disturbances. The duration of the experiment is of 180 sec. As expected, the attenuation depends on the bandwidth of the disturbance.

Figure 11 shows the evolution of the output of the system using YKFIR adaptive feedforward compensator with constant trace adaptation gain for a change in the characteristics of the disturbance at t=180 sec. The first disturbance is a broad band disturbance located between 150 and 250 Hz, while the second one is a broad band disturbance located between 250-350 Hz (the system operates in open-loop for the first 15 sec).

7.4. Experimental Results for FUSBA FIR adaptive compensators

Table 11 gives results obtained with a standard FIR FUSBA compensator for various complexities of the FIR filter on a 180 sec experiment using a broad-band disturbance 150-350 Hz. The FIR filter with 60 parameters has been selected for further investigation.

[14]The lower perfance of the FUPLR and NFULMS algorithms can be explained by the fact that the strictly positive real condition is violated over a significant frequency range.

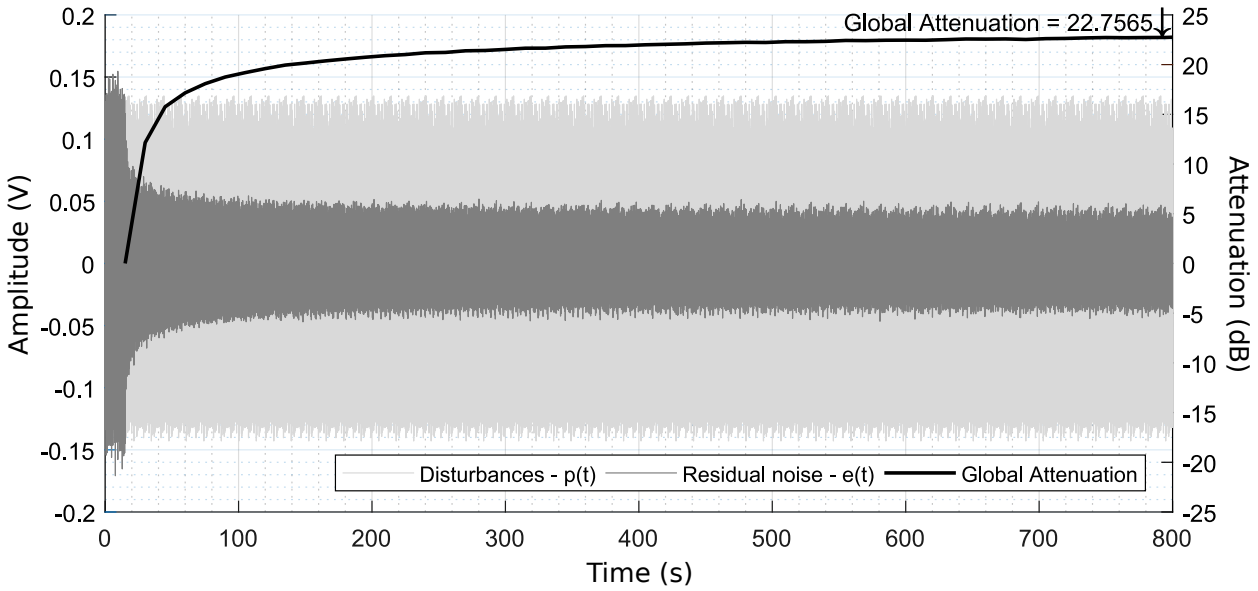

Figure 10: Performance of YKFIR adaptive compensator with 60 parameters (experimental).

Filter type	No. params. [num/den]	Bandwidth	Disturbance	Att. (dB)
YKFIR	60/0	50Hz	150Hz-200Hz	32.33
YKFIR	60/0	50Hz	225Hz-275Hz	33.19
YKFIR	60/0	50Hz	300Hz-350Hz	29.30
YKFIR	60/0	100Hz	150Hz-250Hz	31.68
YKFIR	60/0	100Hz	250Hz-350Hz	23.94
YKFIR	60/0	200Hz	150Hz-350Hz	20.57
YKFIR	60/0	1250Hz	PRBS	5.20

Table 10: Influence of the disturbance characteristics on the performance of the YKFIR adaptive compensator (experimental).

Filter type	No. params.	Attenuation (dB)
FIR	20/0	9.20
FIR	30/0	9.95
FIR	40/0	9.98
FIR	50/0	10.04
FIR	60/0	10.35
FIR	80/0	10.07

Table 11: Influence of the number of parameters on the performance of standard FIR compensator (150-350 Hz broad-band disturbance, 180sec experiment).

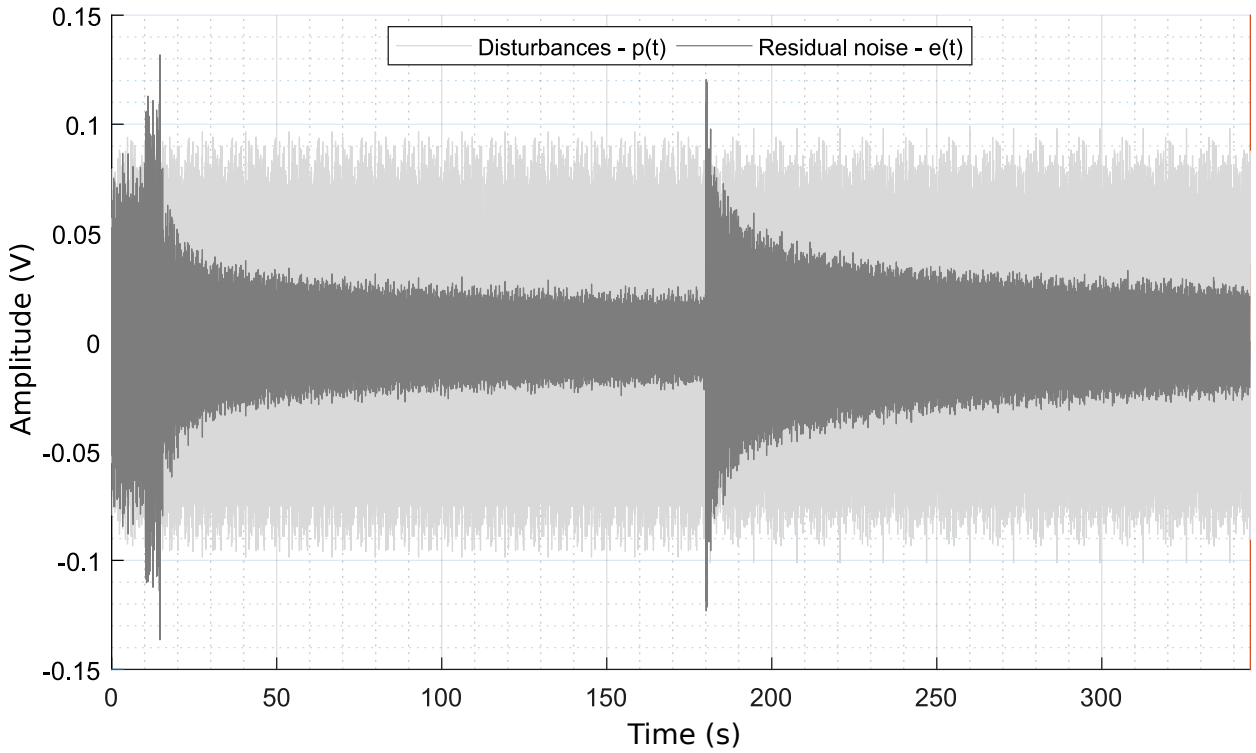

Figure 11: Transient performance of YKFIR adaptive compensator (experimental). 0 to 180s: broad-band disturbance 150-250 Hz; 180 to 345 s: broad-band disturbance 250-350 Hz; open loop operation: 0 to 15 sec.

Nevertheless, the difference observed on this shorter horizon does not allow to conclude clearly for the compromise performance/complexity.

Figure 12 illustrates the performance of the FUSBA FIR using a constant trace adaptation gain over a horizon of 800 sec (60 parameters). One can see that the steady-state operation has not yet been obtained.

Figure 13 shows comparatively the PSD in open-loop and under the effect of the FUSBA FIR compensator and of the FUSBA YKFIR compensator (each with 60 parameters, and the same constant trace adaptation gain with $trace = 60 \times 0.002$). Experiment duration: 800 sec. It can be seen on this figure that the performance of the FUSBA YKFIR is better than the performance of the FUSBA FIR compensator for the same complexity and the same adaptation gain. When using FUSBA FIR scheme, the PSD of the residual noise shows the presence of two very significant picks (around 50 Hz and 450 Hz) correspondng to very low damped poles of the internal closed loop. This questions the robustness of the scheme (instability risk).

8. Conclusions

Based on the experimental and simulation results presented, it can be concluded that the YK-FIR adaptive compensator provides a stable operation and good performance of the adaptive feed-forward active noise compensation system when the delay of the compensator path is larger than

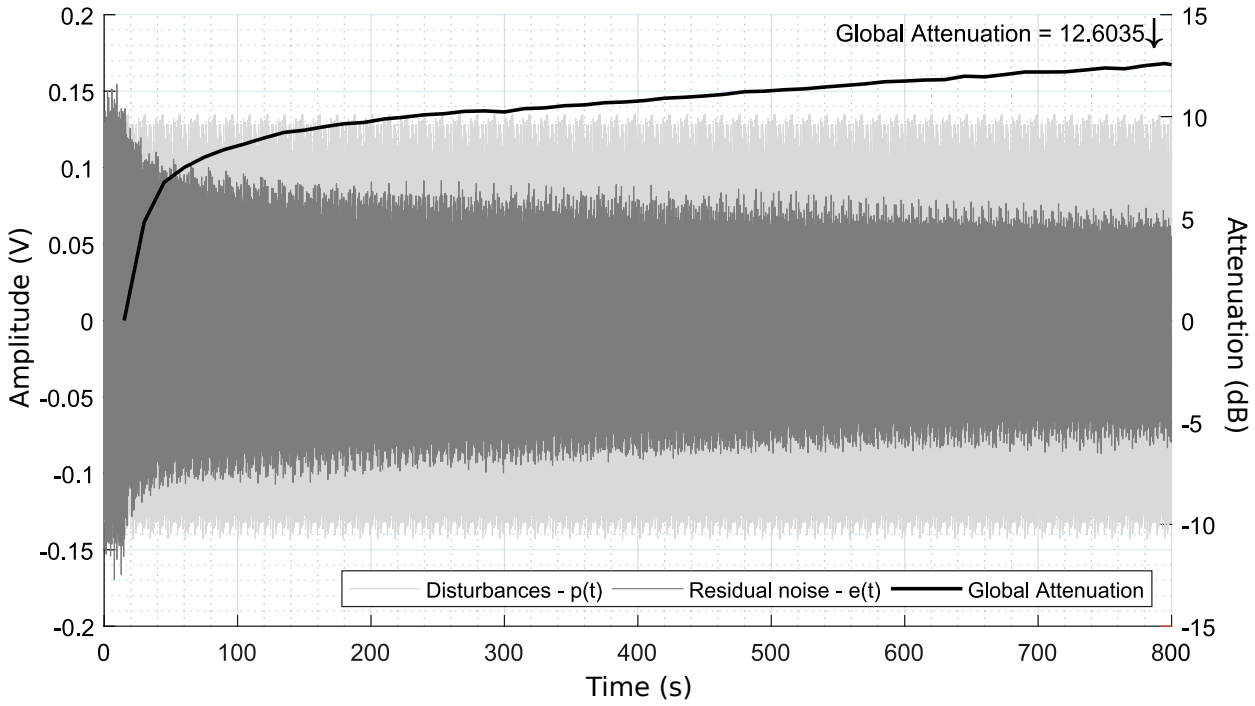

Figure 12: Performance of FUSBA FIR adaptive compensator (60 parameters, experimental).

the delay of the primary path (between the reference source and the residual noise measurement). Its performance is much better than the one of a standard FIR adaptive compensator using the FUSBA algorithm. In addition there are doubts upon the robustness of the FIR adaptive feedforward compensator. The main explanations for this good behavior for the YKFIR adaptive compensator using a FUSBA algorithm are that the internal positive closed-loop will remain stable independently of the values of the adaptive parameters and that the filter to be used for the implementation of the parameter adaptation algorithm is fixed and provides a better approximation of the gradient than the other filtering options used in the various algorithms. Unfortunately, the FULMS and FXLMS algorithms as well as the standard IIR compensators using FUPLR or NFULMS algorithms do not work properly in this configuration (instability). While the YKIIR configuration considered is also unstable, the use of a lattice type algorithms may lead to a stable implementation and this is a subject of further investigation.

Appendix A. Stability/Instability Issues. A Qualitative Analysis

The objective of this appendix is to show that certain adaptive feedforward configurations, in the presence of delay of the secondary path larger than the one of the primary path, present instability risks. One considers the following example:
Primary path:[15] $T = \frac{B_T}{A_T} = \frac{q^{-2}}{1}$.

[15] In some examples, in order to simplify the analysis, we will consider $T = \alpha q^{-2}$.

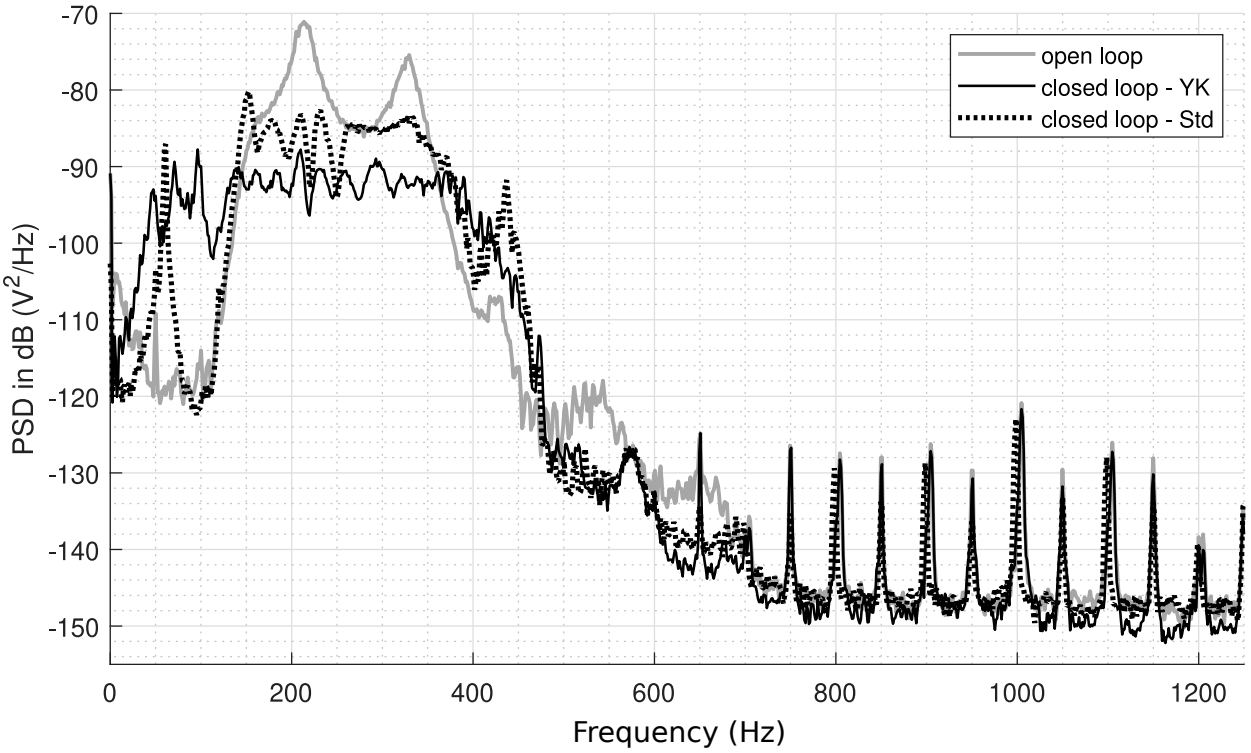

Figure 13: Power spectral density for FUSBA FIR and FUSBA YKFIR (60 parameters, experimental).

Reverse path: $M = \frac{B_M}{A_M} = \frac{q^{-1}}{1}$.

Secondary path: $G = \frac{B_G}{A_G} = \frac{q^{-2}(1+a_{1_G}q^{-1})}{1}$.

The secondary path is characterized by a pure delay of 2 sampling periods and a fractional delay defined by the term $(1+a_{1_G}q^{-1})$ (with a d.c. gain $(1+a_{1_G})$). For $a_{1_G} > 1$, the fractional delay is larger than $0.5T_s$ and the associated zero is unstable (outside the unit circle) [19]. As such, the delay of the secondary path is larger than the delay of the primary path. We will analyse the system for various configurations of the adaptive feedforward compensator.

When "perfect matching" is achieved, we implicitly assume "persistance of excitation", i.e. residual error equal zero implies that parameters converge towards the values assuring perfect matching.

Appendix A.1. IIR adaptive compensator

The IIR adaptive compensator considered has the following structure

$$\hat{N} = \frac{\hat{r}_0}{1+\hat{s}_1 q^{-1}} \tag{A.1}$$

(the time argument has been omitted). The effective compensator constituted by $\hat{N}$ in positive feedback with M will be characterized by the transfer operator:

$$\hat{N}_{CL} = \frac{\hat{r}_0}{1 + (\hat{s}_1 - \hat{r}_0)q^{-1}}. \tag{A.2}$$

The stability of the internal loop requires that the $|\hat{s}_1 - \hat{r}_0| < 1$. The possibility that this value becomes > 1 asymptotically should be avoided.

The compensation path (concatenation of the effective compensator and the secondary path) denoted by C is characterized by the transfer operator:

$$C = \frac{\hat{r}_0 q^{-2}(1 + a_{1_G} q^{-1})}{1 + (\hat{s}_1 - \hat{r}_0)q^{-1}}. \tag{A.3}$$

For perfect matching, one should have

$$\frac{\hat{r}_0 q^{-2}(1 + a_{1_G} q^{-1})}{1 + (\hat{s}_1 - \hat{r}_0)q^{-1}} = -q^{-2}. \tag{A.4}$$

Clearly this can be achieved for $\hat{r}_0 = -1$; $\hat{s}_1 - \hat{r}_0 = a_{1_G}$ and the adaptation mechanism will drive the adjustable parameters towards these values. Therefore for $a_{1_G} > 1$, the internal loop will be unstable.

Appendix A.2. FIR adaptive compensator

The adaptive compensator in this case will have the structure

$$\hat{N} = \frac{\hat{r}_0}{1} \tag{A.5}$$

The effective compensator will be characterized by

$$\hat{N}_{CL} = \frac{\hat{r}_0}{1 - \hat{r}_0 q^{-1}}. \tag{A.6}$$

The compensation path will be characterized by

$$C = \frac{\hat{r}_0 q^{-2}(1 + a_{1_G} q^{-1})}{1 - \hat{r}_0 q^{-1}}. \tag{A.7}$$

For perfect matching one should have (in this case $T = a_{1_G} q^{-2}$)

$$\frac{\hat{r}_0 q^{-2}(1 + a_{1_G} q^{-1})}{1 - \hat{r}_0 q^{-1}} = -a_{1_G} q^{-2}. \tag{A.8}$$

Clearly the equilibrium point will be $-\hat{r}_0 = a_{1_G}$ and the system can become unstable for $a_{1_G} > 1$ (fractional delay larger than $0.5T_s$).

Appendix A.3. YKIIR adaptive compensator

The adaptive compensator has a Youla-Kučera structure with

$$\hat{Q} = \frac{\hat{b}_0^Q}{1 + \hat{a}_1^Q q^{-1}} \tag{A.9}$$

The central controller is characterized by $R_0 = r_0$ and $S_0 = 1$ ($|r_0| < 1$). The compensator will be given by

$$\hat{N} = \frac{(1 + \hat{a}_1^Q q^{-1}) r_0 - \hat{b}_0^Q}{(1 + \hat{a}_1^Q q^{-1}) - \hat{b}_0^Q q^{-1}} \tag{A.10}$$

The effective compensator will be characterized by

$$\hat{N}_{CL} = \frac{(1 + \hat{a}_1^Q q^{-1}) r_0 - \hat{b}_0^Q}{(1 + \hat{a}_1^Q q^{-1})(1 - r_0 q^{-1})}. \tag{A.11}$$

The compensation path will be characterized by

$$C = \frac{\left[(1 + \hat{a}_1^Q q^{-1}) r_0 - \hat{b}_0^Q\right] q^{-2}(1 + a_{1_G} q^{-1})}{(1 + \hat{a}_1^Q q^{-1})(1 - r_0 q^{-1})} \tag{A.12}$$

For perfect matching one should have

$$\frac{\left[(1 + \hat{a}_1^Q q^{-1}) r_0 - \hat{b}_0^Q\right] q^{-2}(1 + a_{1_G} q^{-1})}{(1 + \hat{a}_1^Q q^{-1})(1 - r_0 q^{-1})} = -a_{1_G} q^{-2} \tag{A.13}$$

It can be verified that $\hat{a}_1^Q = a_{1_G}$ and $r_0 - \hat{b}_0^Q = -a_{1_G}$ assure the perfect matching and this equilibrium point corresponds to an internal loop which will be unstable for $a_{1_G} > 1$.

Appendix A.4. YKFIR adaptive compensator

In this case

$$\hat{Q} = \frac{\hat{b}_0^Q}{1}; \qquad R_0 = r_0,\ S_0 = 1 \quad (|r_0| < 1). \tag{A.14}$$

The YKFIR feedforward compensator will be characterized by

$$\hat{N} = \frac{r_0 - \hat{b}_0^Q}{1 - \hat{b}_0^Q q^{-1}} \tag{A.15}$$

The effective feedforward compensator will be characterized by

$$\hat{N}_{CL} = \frac{r_0 - \hat{b}_0^Q}{1 - r_0 q^{-1}}. \tag{A.16}$$

Therefore, the internal closed-loop can not become unstable since the closed loop pole is fixed and depends only upon r_0. This pole is asymptotically stable since $|r_0| < 1$. The transfer operator of the compensation path is characterized by

$$C = \frac{\left(r_0 - \hat{b}_0^Q\right) q^{-2}(1 + a_{1_G} q^{-1})}{1 - r_0 q^{-1}} \tag{A.17}$$

and the perfect matching condition becomes

$$\frac{\left(r_0 - \hat{b}_0^Q\right) q^{-2}(1 + a_{1_G} q^{-1})}{1 - r_0 q^{-1}} = -q^{-2} \tag{A.18}$$

Clearly the "perfect matching" condition can not be achieved for $a_{1_G} > 1$. The error will be characterized by

$$\varepsilon(t) = q^{-2} \left(1 + \frac{\left(r_0 - \hat{b}_0^Q\right)(1 + a_{1_G} q^{-1})}{1 - r_0 q^{-1}} \right) p(t) \tag{A.19}$$

The adaptation will try to minimize the error, but the internal loop will remain stable for all possible values of $\hat{b}_0^Q$. Augmenting the order of $\hat{B}_Q$ will allow to further reduce the error but the internal loop will remain stable.

Conclusion: This qualitative analysis has shown that for the case where the delay of the secondary path exceeds by more than $0.5T_s$ the delay of the primary path, the risk of instability occurs for IIR, FIR and YKIIR feedforward compensators. For the YKFIR this risk does not exist and the poles of the internal loop are fixed and defined by the central controller.

Appendix B. A simplified YKFIR adaptive compensator

Choosing $R_0 = 0$ and $S_0 = 1$ for the central controller, the FUPLR, NFULMS, FUSBA and SFUSBA adaptation algorithms will use the same filter $L = \hat{G}$ (since in this case $P = A_M$) and the stability condition becomes : "$G/\hat{G} - \lambda/2$ should be strictly positive real" (where $\lambda = 0$ for scalar adaptation gain). The parameters will be adapted using Eq. (16) with **k(t)** given by Eq. (15) for a matrix adaptation gain and by Eq. (20) for a scalar adaptation gain. From Eq. (29) it results that in this case the control $\hat{u}(t+1)$ is given by :

$$\hat{u}(t+1) = \hat{u}(t+1|\hat{\mathbf{w}}(t+1)) = \hat{\mathbf{w}}^T(t+1)\mathbf{u}(t) \tag{B.1}$$

A YKFIR compensator with 60/0 parameters has been considered for simulations. A disturbance with a flat spectrum between 150 and 350 Hz has been used as disturbing noise. Figure B.14 gives the time evolution of the residual noise for the case of a matrix adaptation gain with constant trace (trace=60). Figure B.15 gives the time evolution of the residual noise for the case of a scalar adaptation gain with a constant trace of 60 (i.e. a scalar gain $\gamma = 1$. Figure B.16 shows the comparison between the PSD for the two adaptation schemes. the corresponding PSD (computed for the last 10s of the simulation). A global attenuation of 24.32 dB is obtained for the matrix algorithm and 22.86 dB for the scalar one.

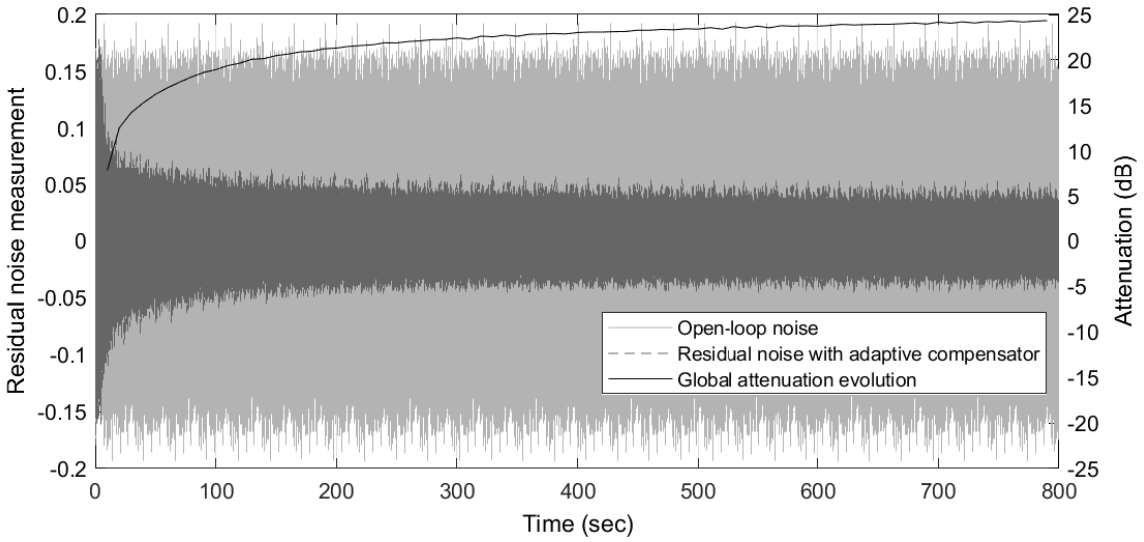

Figure B.14: Time domain evolution of the residual noise for the YKFIR 60/0 simplified adaptative compensator with matrix adaptation gain (constant trace of 60).

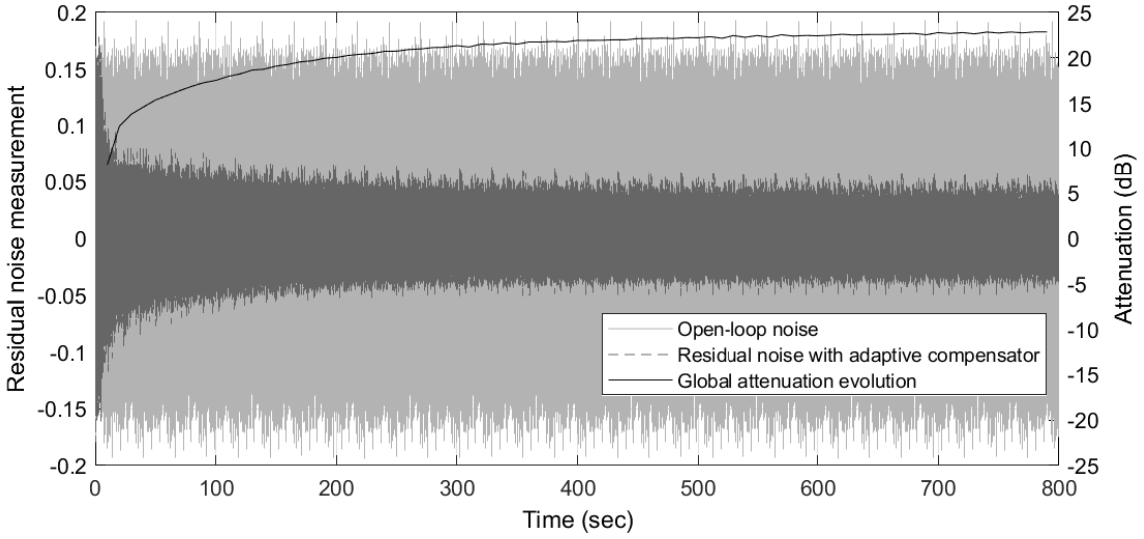

Figure B.15: Residual noise of the YKFIR 60/0 adaptation compensator with scalar gain (constant trace of 60, gain per parameter: 1).

References

[1] C. Jacobson, J. Johnson, C.R., D. McCormick, W. Sethares, Stability of active noise control algorithms, Signal Processing Letters, IEEE 8 (3) (2001) 74 –76.

[2] I. Landau, M. Alma, T. Airimitoaie, Adaptive feedforward compensation algorithms for active vibration control with mechanical coupling, Automatica 47 (10) (2011) 2185 – 2196.

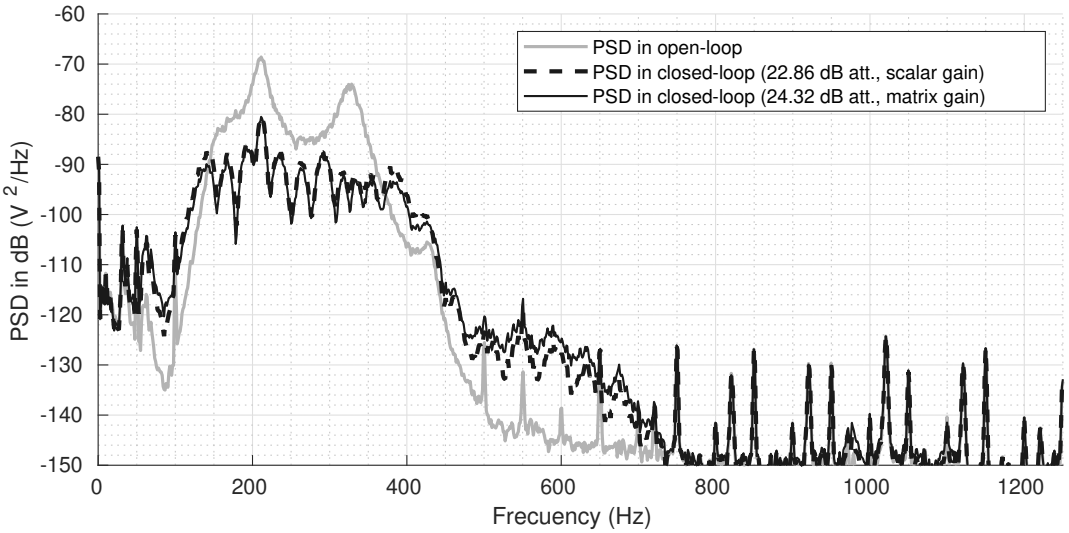

Figure B.16: PSD estimate of the YKFIR 60/0 adaptation compensator with scalar and matrix adaptation gains (constant trace of 60).

[3] I. D. Landau, T.-B. Airimitoaie, M. Alma, A Youla–Kučera parametrized adaptive feedforward compensator for active vibration control with mechanical coupling, Automatica 48 (9) (2012) 2152 – 2158.

[4] S. Elliott, Signal processing for active control, Academic Press, San Diego, California, 2001.

[5] J. Zeng, R. de Callafon, Recursive filter estimation for feedforward noise cancellation with acoustic coupling, Journal of Sound and Vibration 291 (3-5) (2006) 1061 – 1079.

[6] R. Fraanje, Robust and fast schemes in broadband active noise and vibration control, Ph.D. thesis, University of Twente, Twente, The Netherlands (2004).

[7] J. Hu, J.-F. Lin, Feedforward active noise controller design in ducts without independent noise source measurements, IEEE Trans. on Control System Technology 8 (3) (2000) 443–455.

[8] I. D. Landau, T.-B. Airimitoaie, A. Castellanos Silva, A. Constantinescu, Adaptive and Robust Active Vibration Control—Methodology and Tests, Advances in Industrial Control, Springer, London, 2017.

[9] R. Melendez, I. Landau, L. Dugard, G. Buche, Data driven design of tonal noise feedback cancellers, in: Proceedings of the 20th IFAC World Congress, Toulouse, France, 2017, pp. 916–921.

[10] M. Kuo, D. Morgan, Active noise control systems-Algorithms and DSP implementation, Wiley, New York,, 1996.

[11] S. Kuo, D. Morgan, Active noise control: a tutorial review, Proceedings of the IEEE 87 (6) (1999) 943 – 973.

[12] I. D. Landau, R. Lozano, M. M'Saad, A. Karimi, Adaptive control, 2nd Edition, Springer, London, 2011.

[13] S. Haykin, Adaptive Filter Theory, Prentice Hall, Englewood Cliffs N.J., 1996.

[14] L. Eriksson, Development of the filtered-U LMS algorithm for active noise control, J. of Acoustical Society of America 89 (1) (1991) 257–261.

[15] B. Widrow, D. Shur, S. Shaffer, On adaptive inverse control, in: Proc. 15th Asilomar Conf. Circuits, Systems and Computers, Pacific Grove, CA, USA, 1981.

[16] I. D. Landau, T.-B. Airimitoaie, M. Alma, IIR Youla–Kučera parameterized adaptive feedforward compensators for active vibration control with mechanical coupling, IEEE Transactions on Control System Technology 21 (3) (2013) 765–779.

[17] P. Regalia, Adaptive IIR Filtering in Signal Processing and Control, Dekker, New York, 1995.

[18] J. Lu, C. Shen, X. Qiu, B. Xu, Lattice form adaptive infinite impulse response filtering algorithm for active noise control, The Journal of the Acoustical Society of America 113 (1) (2003) 327–335.

[19] I. Landau, G. Zito, Digital control systems – Design, identification and implementation, Springer, London, 2005.